Thermophysics and Aeromechanics, *2016*, *Vol. 23*, *No. 3*

DOI: 10.1134/S0869864316030033

Conventional measuring probes in the wall layer of turbulent subsonic ducted flows

E.-S. Zanoun[1,2], E. Öngüner[3], and C. Egbers[3]

[1]*American University in Cairo*, *New Cairo*, *Egypt*

[2]*Benha University*, *Benha*, *Egypt*

[3]*Brandenburg University of Technology*, *Cottbus-Senftenberg*, *Germany*

E-mail: elsayed.zanoun@bhit.bu.edu.eg

(*Received February 5*, *2015*; *in revised form March 17*, *2015*)

This piece of work is concerned with the application of two conventional measuring probes, pressure probe and hot wire, in the wall layer of subsonic ducted, pipe and channel, flows for velocity measurements. Careful measurements have been carried out and analysed accordingly for Reynolds number range of $2.8\times10^5\le Re_m\le4.5\times10^5$ and $4\times10^4\le Re_m\le2.3\times10^5$ for the pipe and the channel, respectively. Pressure probes of outer diameters ($d_0^+ = d_0\cdot u_\tau/\nu$) 20–120 wall units and hot wire, having wire length ($l^+ = l\, u_\tau/\nu$) of 50–250 for the current Reynolds range, have been utilized to carry out the present measurements. When the pressure probe was applied in the wall layer, the wall proximity and the shear gradient played major roles of its incorrect velocity readings, however, this effect was far from being influencing the hot-wire velocity measured in the overlap region. When the pressure probe results compared to those obtained by the hot wire, the pressure probe's data showed hump in the normalized mean velocity profiles around the wall distances $y^+\le300$ and $y^+\le150$ for the pipe and the channel, respectively. Available corrections are adopted and applied to the pressure probe data measured, yielding results that are comparable to those of the hot wire and this was also demonstrated by comparing the present results corrected to the so-called the logarithmic velocity profile.

Key words: hot wire, pressure probe correction, pipe and channel flows.

Introduction

Local turbulence properties in ducted flows, i.e., pipes and channels, are of importance in turbulence modelling as well as in engineering applications. Variety of conventional and advanced available measuring techniques, e.g., thermal (hot wire/film), pressure (Pitot & Pitot-static), and optical (laser-Doppler anemometry), probes, having finite measuring volumes, are usually in common use to carry out such local turbulence measurements. Some of these techniques provide volume-average information about the turbulent flow characteristics that might affect conclusions drawn from the resultant data. Moreover, errors in the data measured, utilizing such pressure probes and hot wires, due to viscous effects, interference effects and temperature drift are expected. Calibration of the hot-wire probe prior to its employment to conduct the turbulent flow measurements is also of prime importance. Hence, small sizes of the measuring volumes of those measuring techniques are to be chosen such that the shear

gradient and interference effects is minimal, in particular, in the wall region to obtain accurate local measurements. Corrections for the viscous, shear, wall-proximity, and turbulence effects are therefore to be carried out for the pressure probes. Accurate calibration curve and constant-temperature working medium are also required for utilizing the hot wire. The present paper is, therefore, concerned with measurements of the local mean properties of fully developed turbulent pipe and channel flows utilizing the pressure probe and the hot wire. It outlines also some correction methods that are known to pressure probes, yielding local accurate data from both measuring probes. The mean-flow local information corrected from both measuring techniques is of importance, for instance, in frictional drag estimation as well as for evaluating the logarithmic law of the wall. To obtain such reliable information, well designed test rigs are needed, yielding flow with the required fully developed properties. Two test facilities, i.e. pipe and channel, were set up and utilized to carry out such measurements. A carefully designed pipe flow facility was constructed at the Department of Aerodynamics and Fluid Mechanics (LAS), Brandenburg University of Technology (BTU-Cottbus-Senftenberg), providing the desired fully developed pipe flow characteristics [1]. On the other hand, the channel flow facility at the Institute of Fluid Mechanics (LSTM), Erlangen Nürenberg [2] was utilized. Both facilities use air as a working fluid medium. Intensive measurements using pressure probes, having outer diameters d_0 of 0.6 mm, and 1 mm ($d_0^+ = d_0 \cdot u_\tau / \nu$ =20–120 wall units) have been carried out. In addition, new data measured with high enough spatial resolution were obtained by investigating the turbulent pipe and channel flows at LAS and LSTM utilizing the hot wire, having small measuring volume, i.e., wire diameters (d) of 3.8 and 5 μm and wire lengths l of 760 and 1250 μm, respectively. In terms of wall units, the hot-wire length ($l^+ = l\, u_\tau / \nu$) was ranging from 50 to 250, for the current Reynolds number working range, $2.8\times10^5 \le \mathrm{Re_m} \le 4.5\times10^5$, and $4\cdot10^4 \le \mathrm{Re_m} \le 2.3\cdot10^5$, for the pipe and the channel, respectively. Hereafter, the Reynolds number is defined as $\mathrm{Re_m} = D\overline{U}_\mathrm{b} / \nu$, where $\overline{U}_\mathrm{b}$ is the bulk flow velocity, D is the pipe inner diameter and/or the channel full height (i.e., $D \equiv H$), and ν is the air kinematic viscosity.

The pipe experimental facility and the applications of the measuring techniques utilized are introduced briefly in section 2. Selected methods adopted from the literature for correcting the pressure probe measurements for the wall proximity and the shear gradient are described in section 3. In addition, a comparative study between the hot wire and the pressure probe results was conducted. Conclusions and outlooks are presented in the final section.

Experimental facility and procedures

The main objective of the present work is to obtain detailed experimental data from two different duct facilities, having circular and rectangular cross sections and utilizing two measuring techniques. The first facility is called the CoLaPipe. It is a pipe facility built at the Department of Aerodynamics and Fluid Mechanics (LAS) at the Brandenburg University of Technology (BTU-Cottbus-Senftenberg). It is worth noting here that the CoLaPipe is participating in the program "**Eu**ropean **H**igh-Performance **I**nfrastructures in **T**urbulence," **EuHIT**. The LAS **CoLaPipe** (**Co**ttbus **La**rge **Pipe**) shown in Fig. 1 is a relatively high Reynolds number test facility for various purposes ranging from basic to applied researches [1]. It is closed-return facility with the suction side made of high-precision smooth Acrylic glass, having an inner pipe diameter (D_in) of 190±0.23 mm and total length (L) of 28 m, i.e., $L/D_\mathrm{in} \approx 148$. The suction section has an inlet contraction (CR) equals to 9.9 and the expansion ratio (ER)

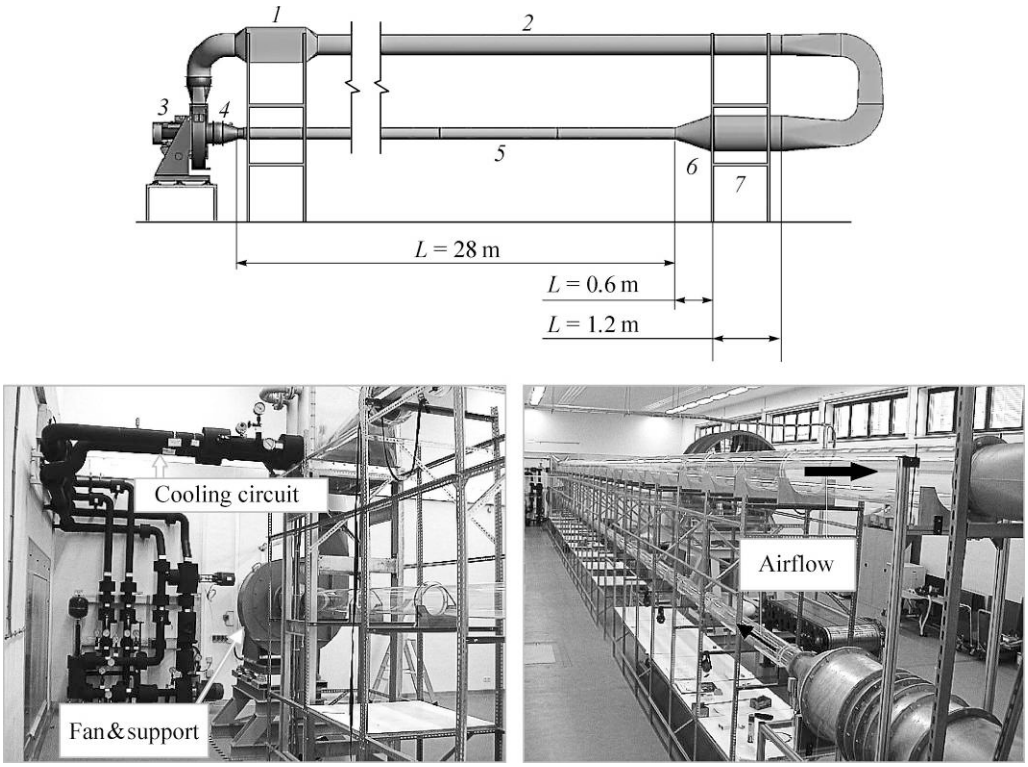

Fig. 1. The CoLaPipe facility at the Department of Aerodynamics and Fluid Mechanics (LAS BTU Cottbus-Senftenberg).

1 — cooling unit: $P = 45$ kW, *2* — return line: $D_{in} = 0.342$ m, $L/D = 79$, $Re_m \le 5 \cdot 10^5$,
3 — blower: $P = 45$ kW, $p = 9.5$ kPa, *4* — diffusor: $D_{in} = 0.19$ m, $D_{exit} = 0.335$ m, $L = 0.335$ m, ER = 3.4,
5 — pipe test section: $D_{in} = 0.19$ m, $L/D = 148$, $Re_m \le 10^6$, $R^+ \le 18.5 \cdot 10^3$,
6 — inlet contraction: $D_{in} = 0.6$ m, $D_{exit} = 0.19$ m, $L = D_{in}$, CR = 9.9,
7 — settling chamber: $D = 0.6$ m, $L = 1.2$ m.

at the diffuser end equals to 3.4. The facility has a return pipe section made also of smooth Acrylic glass with an inner diameter of 342±0.32 mm, and having $L/D \approx 79$. The facility is equipped with water cooler to keep the air temperature constant inside both pipe test sections, i.e., the suction and the return lines. The air temperature was measured within an accuracy of ±0.05 °C. The pipe facility utilizes a powerful 45 kW radial blower to provide air with 80 m/s maximum speed at the contraction exit with turbulence level less than 0.5%. The maximum air speed achieved within the setup corresponds to 0.23 Mach number, avoiding any compressibility effects (i.e., the maximum percentage change in air density was found to be 0.06% corresponding to the Mach number of 0.23). Aiming at a quite stable facility, the radial blower is located at the end of the pipe test section in the suction side and delivers its output to the 342 mm diameter return line through a heat exchanger as shown in Fig. 1. A computer controlled three dimensional high spatial resolution traverse system (isel®Germany AG) was in use for traversing both the pressure probes and the hot wire. The traverse is placed on scaled rail to facilitate its movement in streamwise, spanwise, and normalwise directions. The positioning absolute error with the traverse mechanism is around ±10 μm. An approach adopted by [3] was applied with enough care to ensure precise location of the hot wire inside the pipe test section. On the other hand, the pressure probe's first measuring location was determined when the pressure probe was resting on the pipe/channel wall, providing a reference for the distance measured from the wall surface. For further details about the relevant components of the facility the reader is directed to references [1] and [4].

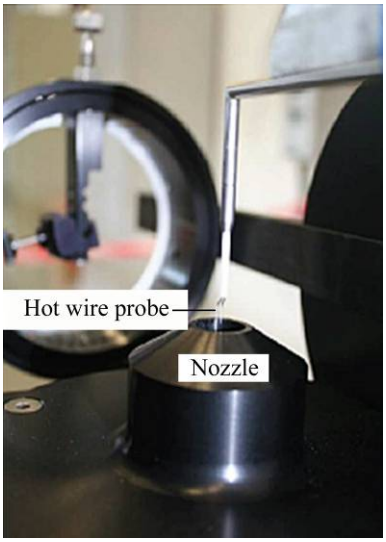

Fig. 2. Dantec calibration unit with the HWA probe.

In addition to the pipe facility, some new channel flow data were obtained and presented, utilizing the channel flow test facility at LSTM Erlangen, see [2] for the channel details. The mean velocity profiles and the mean wall pressure gradients along the pipe and the channel test sections have been measured for various Reynolds numbers. All the pipe velocity profiles-measured were carried out at a downstream distance of 130D from the pipe contraction exit. While the measuring location for the channel flow was taken at a distance of 115H from the channel inlet [2]. These lengths were considered sufficient to ensure fully developed turbulent pipe and channel flows by reaching the measuring test sections [5].

The present velocity profile measurements using the hot wire were conducted using the 3.8-μm diameter wire, the TSI probe, and anemometer. In addition, few runs have been carried out using the 5-μm diameter wire mounted on Dantec Constant Temperature Anemometer (CTA). All wires have aspect ratio of $l/d \geq 200$, i.e., the length of the active part of the sensor is 200 the wire diameters, assuring the two dimensionality and negligible prongs effect. The hot-wire probes were calibrated before each set of measurements utilizing the Dantec calibration unit shown in Fig. 2. All calibrations and measurements were performed with an 80 % overheat ratio. A fourth-order polynomial fit was the basis for the mean velocity estimation with accuracy better than ±1 %. The ambient air temperature inside the pipe/channel test sections was kept constant. In case of an unavoidable temperature drift, instantaneous corrections were carried out during the calibration procedure as well as during measurements only for temperature drifts not greater than ±1 %. Data with temperature drifts greater than ±1% were excluded from the current analysis.

The pressure probe velocity measurements were made by traversing total-head probes, having inner diameters d_i = 0.25 mm and 0.6 mm. All pressure probes were designed each with an inner-to-outer diameter ratio between 0.5 and 0.6 in accordance with recommendations made by [6–8]. The dynamic head needed for velocity calculation was obtained by subtracting the static pressure measured using a wall tap of inner diameter 0.4 mm from the total pressure measured by the total head probe. It is worth noting that the static pressure tap was located at the same downstream location as the tip of the total heat probe. Utilizing the Bernoulli equation, the pressure probe measurements were then converted to velocity. Each velocity profile was measured at around 70 vertical positions with particular care being given to the velocity distribution within the so-called the overlap region.

Results and analysis

Pipe and channel wall frictions

The two experimental facilities and measuring techniques, described in the previous section, enabled obtaining reliable mean velocity and wall friction data for fully developed turbulent flows in both facilities. The wall friction velocity u_τ and the wall distance are essential parameters to measure, accurately, to investigate reliably both flows. The wall friction velocity was obtained via a careful estimation of the wall shear stress by measuring the mean pressure gradient (dP/dx) along the pipe and/or the channel centerlines, see Fig 3.

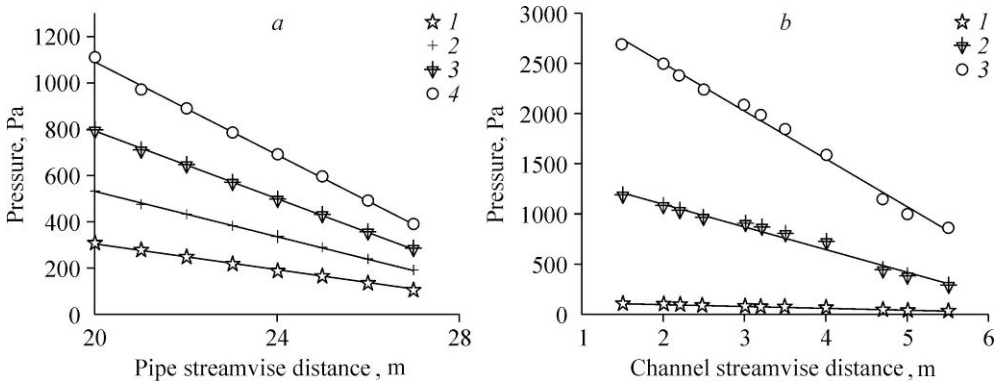

Fig. 3. Samples from the mean pressure gradients along
(*a*) the pipe wall and (*b*) the channel centrelines.
a — R^+ = 4576 (*1*), 6021 (*2*), 7342 (*3*), 8652 (*4*), *b* — R^+ = 1014 (*1*), 3487 (*2*), 4780 (*3*).

To obtain the mean pressure gradient, the mean static pressure was measured far enough from the pipe inlet at four different pressure locations, starting at $L/D \approx 100$, all being 1 m apart from each other. At each measuring location, three static pressure taps of 400-μm diameter were carefully installed around the circumference of the pipe. After checking the readings agreement among the three pressure points at each measuring location, the mean static pressure was obtained by averaging the readings of the agreed pressure taps. After checking the readings agreement among the three pressure points at each measuring location, the mean static pressure was obtained by averaging the readings of the agreed pressure taps. Thereafter the mean pressure gradient along the seven meters was estimated with accuracy better than ±0.25 %. A similar approach was carried out for the channel flow. The wall friction velocity (u_τ) was then estimated:

$$u_\tau = \sqrt{\tau_\mathrm{w} / \rho}, \qquad \tau_\mathrm{w} = -\frac{R}{2}\cdot\frac{dP}{dx} \text{ — (pipe)}, \quad \tau_\mathrm{w} = -\frac{H}{2}\cdot\frac{dP}{dx} \text{ — (channel)}, \tag{1}$$

where R is the pipe radius and H is the channel full height. Then, the pipe friction factor, λ, and the channel skin friction coefficient, c_f, respectively, can be written as:

$$\text{Pipe friction factor} — \lambda = 8\left(u_\tau / \overline{U}_\mathrm{b}\right)^2, \qquad \text{Channel skin friction coefficient} — c_\mathrm{f} = 2\left(u_\tau / \overline{U}_\mathrm{b}\right)^2. \tag{2}$$

It is worth noting here that the static pressure was measured using wall tapping of finite measuring diameter, and therefore a Reynolds-number-dependent correction for the static pressure readings might be needed. However, corrections for the finite static pressure tap diameter (d) were found to be negligible if $d^+ < 50$ according to [9]. For the current analysis, this correction was neglected since the diameter of the pressure taps in both experiments, i.e. the pipe and the channel, was 400 μm, in terms of wall units was in the range $15 < d^+ < 55$.

Having a universal equilibrium range of energy spectrum versus the wave number, i.e., generalization of the Kolmogorov –5/3 law of turbulence, a real inertial sublayer, and a well-established friction relationship $\lambda = f(\mathrm{Re})$, that follows the Prandtl–von Kármán logarithmic friction relation [10] are to be considered to assure high Reynolds number pipe facility. As expected for the fully developed turbulent pipe flow at relatively high enough Reynolds numbers, the pipe friction data obtained from the current pressure gradient measurements, presented in Fig. 3, compared well with available friction relations [10–11], and experimental data [12–13] as shown in Fig. 4, fulfilling criteria of flow full development discussed earlier.

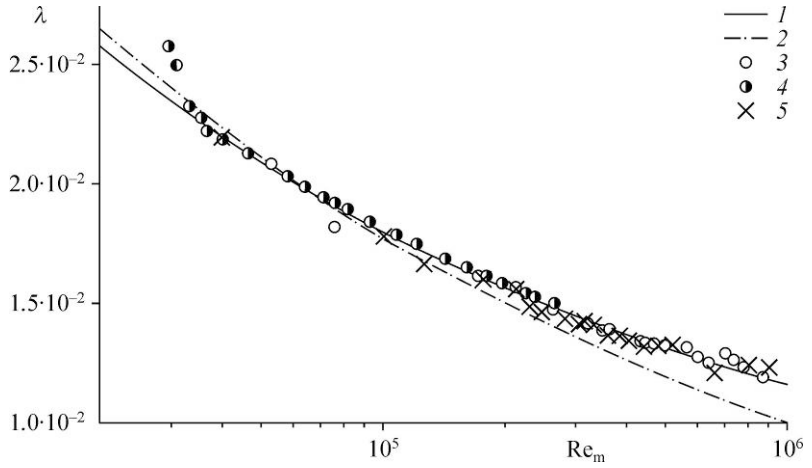

Fig. 4. Present pipe friction data compared with data and formulae extracted from the literature. *1* — [10]: $1/\sqrt{\lambda} = 2\log(\mathrm{Re}_m\sqrt{\lambda}) - 0.8$, *2* — [11], *3* — [12], *4* — [13], *5* — present smooth pipe.

A reasonable agreement was observed in Fig. 4 with the Prandtl–von Kármán logarithmic friction relation $1/\sqrt{\lambda} = 2\log\cdot\left(\mathrm{Re}_m\sqrt{\lambda}\right) - 0.8$, and with the smooth pipe experimental data of [12] and [13]. A good agreement with [11] was obtained, however, for $\mathrm{Re}_m < 10^5$.

In channel flow, reliable wall skin friction data requires the validity of the assumption that the mean flow statistics are two dimensional. The flow two-dimensionality is connected with the so-called channel aspect ratio (*W/H*), i.e. the ratio of the channel width (*W*) to the channel full height (*H*). A minimum aspect ratio of five to assure the flow two dimensionality was proposed by [14]. On the other hand, a recommended minimum aspect ratio of eight was proposed by [15] to avoid the channel side-wall effects. More recently, [16] stated that an aspect ratio greater than ten is required to minimize the channel side-wall effects on the centerline wall shear measurements. The set of the data selected and presented in Fig. 5 have been obtained utilizing channels having aspect ratios greater than 10, satisfying flow two dimensionality criteria.

Figure 5 shows that the present wall skin friction data obtained from the mean-pressure gradient measurements along the channel centerline compare well with the wall skin friction data obtained using the oil film interferometry as well as with the logarithmic skin friction relation proposed by [2]. Few skin friction experimental data sets [17–19] for the channel flows are also presented in Fig. 5. The data set of [17] were obtained via the mean-pressure gradient measurements in plane channel, having an aspect ratio of 11.7:1 for relatively high Reynolds number ($\mathrm{Re}_m < 2\cdot10^5$). Good agreement was observed among the various experimental data sets and with the logarithmic skin friction relation proposed by [2], in particular, for $R^+ \geq 2000$, where $R^+ = Hu_\tau/2\nu$ which is equivalent to $\mathrm{Re}_m = 86000$.

Pressure probe versus hot wire velocity profiles

In addition to the experimental data of the wall friction discussed above, the cross-sectional mean velocity profile was measured with enough care for different values of Reynolds numbers, utilizing the total pressure probe. It is, however, known that the presence of a pressure probe in the wall layer of the wall-bounded shear flows causes changes in flows nature, see, e.g., [20], which can be summarized as follows:

1. Viscous effect: this effect is to be taken into consideration when $\mathrm{Re}_p < 200$, where Re_p is the Reynolds number defined based on the probe outer diameter d_0 and the bulk flow velocity.

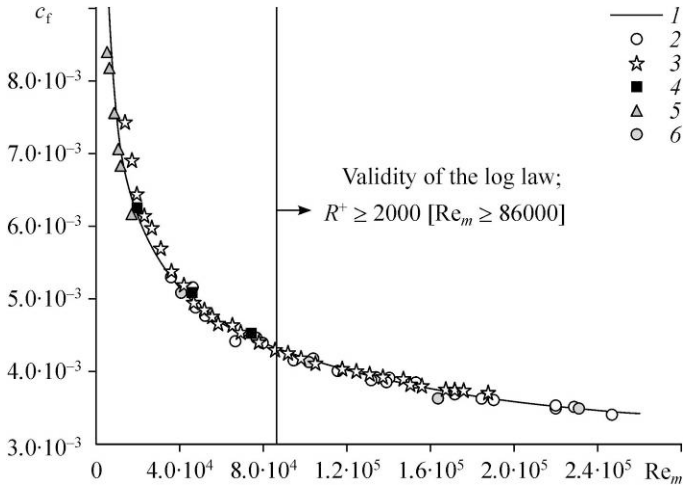

Fig. 5. Present channel skin friction data compared with the logarithmic friction relation proposed by [2] and with data extracted from the literature.

1 — computation of [2]: $W/H = 12$, $1/c_f = 1.911 \ln(\mathrm{Re_m}\sqrt{c_f}) - 1.282$; *2* — experiment of [2]: $W/H = 12$; *3* — [17]: $W/H = 11.7$; *4* — [18]: $W/H = 10$; *5* — [19]: $W/H = 18$; *6* — present smooth channel: $W/H = 12$.

2. Wall proximity effect (i.e., velocity profile distortion near a solid boundary): it is to be observed when the pressure probe is located within two-to-three probe diameters (i.e., $y < 2–3\ d_0$) from the wall surface.

3. Velocity/shear gradient or displacement effect: this effect is due to

– the deflection of the incoming streamlines by the pressure probe under the velocity gradient when the probe is located at wall distance $y > 2\ d_0$;

– the in-equability of the average pressure measured by the pressure probe face to the pressure measured at the geometric center of the probe, see [20] for more details.

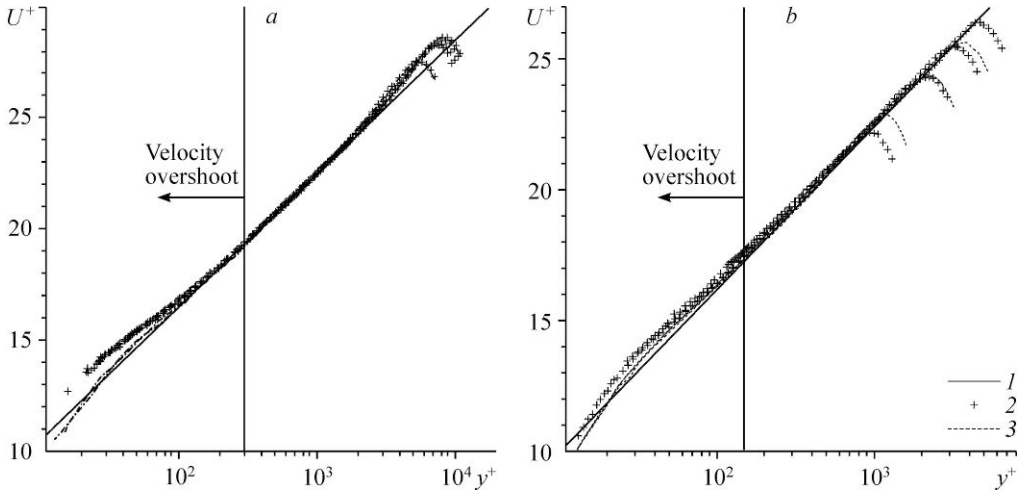

Fig. 6. Uncorrected mean velocity profiles from pressure probes in comparison to the hot wire and the logarithmic lines in (*a*) pipe, and (*b*) channel flows.

1 — logarithmic line: $k = 0.384$, $B = 4.43$ (*a*), $k = 0.37$, $B = 3.7$ (*b*);

2 — Pitot data, uncorrected: $R^+ = 5711–8652$, ($d_0^+ = 45–70$) (*a*), $R^+ = 1014–4816$ ($d_0^+ = 24–116$) (*b*);

3 — hot wire data: $R^+ = 5575–8509$ (*a*); $R^+ = 1167–3900$ (*b*).

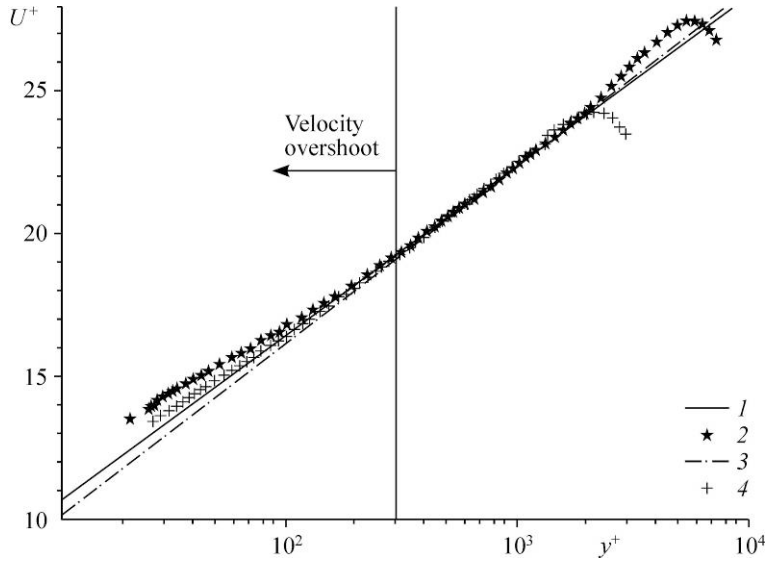

Fig. 7. Uncorrected mean velocity profiles from pressure probes in the pipe and the channel flows.

1 — pipe Log line: $k = 0.384$, $B = 4.43$; *2* — Pitot pipe data, uncorrected: $R = 5711$ ($d_0^+ = 61$);

3 — channel Log line: $k = 0.37$, $B = 3.7$; *4* — Pitot channel data, uncorrected: $R^+ = 2302$ ($d_0^+ = 55$).

Of the three effects listed above, the velocity/shear gradient effect is the most noticeable effect in the wall-bounded shear flows. It has been the goal of a number of earlier and recent investigations, see e.g. [8, 20–24], to correct pressure probes in the wall layer of turbulent flows. The correction for the viscous effect is, however, to be taken into consideration when $30 < \mathrm{Re_p} < 200$ as recommended by [20]. For the present measurements, the lowest Reynolds number value achieved is beyond the upper limit criteria, i.e., $\mathrm{Re_p} = 200$, assumed for the viscous effect, and thus corrections for the viscous effect were neglected. On the other hand, a correction for the distortion of the velocity profile, i.e. the wall proximity effect, in the wall vicinity has been taken into account to compensate for the blockage effect caused by the measuring probe [20–24]. The presence of the pressure probe in the wall proximity causes asymmetry of the incoming streamlines and results in the measured total pressure at the probe position to be greater than that for flow in absence of the probe in flow field.

To better analyze the influence of the probe size on the mean velocity, the measured data is to be expressed in terms of the wall units. Hence, the wall friction velocity, u_τ, and the viscous length, $l_\mathrm{c} = \nu / u_\tau$, scales were used to represent the results in general form, i.e. representing the mean velocity distribution in the form of $U^+ = f(y^+)$, where $U^+ = U / u_\tau$ and $y^+ = y / l_\mathrm{c}$. Selected samples of the uncorrected probe mean velocity profiles in both the pipe, Fig. 6*a*, and the channel, Fig. 6*b*, flows are illustrated and compared with the hot-wire data for similar Reynolds numbers. It is of importance to report here that the wall thermal conductivity effect on the measured velocity using the hot wire appears for wall distances below $y^+ = 5$, owing to the additional heat losses from the wire caused by the wall conductivity, e.g. see [3]. This effect was far from being affecting the current hot-wire measurements since the closest measuring location was for wall distances $y^+ > 10$. Velocity overshoots were clearly observed in the region where $y^+ < 300$ in the pipe and for $y^+ < 150$ in the channel, resulting in disagreement between the pressure probe and the hot-wire data in wall proximity. On the other hand, one might observe that the measured velocity profiles by the pressure probe for $y^+ > 300$ in the pipe, and for $y^+ > 150$ in the channel showed satisfactory agreement with the hot-wire data along the overlap and the core regions and with the following logarithmic line:

$$U^+ = \frac{1}{\kappa}\ln y^+ + B \tag{3}$$

having $\kappa = 0.384$ and B=4.43 for the pipe flow with log interval $y^+ = 300–0.15R^+$ [25], and $\kappa = 0.37$ and $B = 3.7$ for the channel flow with log interval $y^+ = 150–0.2R^+$ [2].

The pressure probe produces overshoot in the mean velocity distribution in both the pipe and the channel flows when the measuring probe is located around the buffer region, i.e., $5 < y^+ < 300$, as can be seen from both Figs. 6 and 7. One could observe from both figures and in particular from Fig. 7 a weaker velocity overshoot in the channel flow than that in the pipe flow which might be attributed to the fact that the inner-region structure for the pipe flow is more complex than in the channel flow.

To clarify the wall effect on the mean velocity profile measured, Fig. 8 is a simple depiction illustrating rectangular and circular duct-cross sections. One expects for a channel having high enough aspect ratio ($W/H \geq 10$) a negligible side wall effects on the core flow structure, see [16]. It might be also speculated that in plane-channel flow there is elementary vortices interaction from the opposing walls, simply forming less-complex flow structure in the core region, and therefore less influencing the inner-region flow structure. On the other hand, from infinite number of circumference locations from the pipe interior surface there are interchanges of counter-rotating vortices towards the pipe core, strongly influencing the flow structure in the inner region as well as in the core of the pipe flow, see [26] for more details. This results in some remarkable flow differences between the two ducted flow, i.e., rectangular channel and circular pipe, in both the wall and the core regions.

The velocity overshoot observed in the pipe flow in both Figs. 6 and 7 was interpreted by [27] as part of the mean velocity distribution which can be represented by a power law. On the other hand, the velocity overshoot obtained in the channel flow by [28] with the utilization of the laser Doppler anemometry was interpreted as an effect of the low Reynolds number, making the data to departure from the logarithmic velocity profile. Discrepancies up to 12 % was observed between the pressure probe and the hot wire data obtained around the buffer region, i.e., $y^+ < 30$, in agreement with observation made earlier by [24]. The departure level of the pressure probe data measured from the hot-wire data depends mainly on the size of the measuring volume of the pressure probe as well as on the probe proximity from the wall. This departure, i.e., the overshoot observed in velocity profiles, might be a reasonable justification for the higher value of the slope, i.e. the von Kármán constant, of the logarithmic velocity profile obtained when the pressure probes are being used for velocity measurements, in particular, if the inner limit of the log line is being taken as $y^+ = 30$, see Tables 1 and 2.

To have reliable pressure probe measured data, in particular, when the probe is placed in close proximity to walls, it is believed that corrections are to be applied, see, e.g., [20–24]. Variety of corrections for pressure probe readings are available in the literature that can be applied to make its readings in close agreement with probes of small measuring volumes such as hot wire and laser Doppler. Corrections for the wall proximity, the displacement (i.e. shear gradient), and the wall turbulence were carried out for various Reynolds numbers, i.e., $2.8\cdot10^5 \leq \leq \mathrm{Re_m} \leq 4.5\cdot10^5$ and $4\cdot10^4 \leq \mathrm{Re_m} \leq 2.3\cdot10^5$, for the pipe and the channel flows, respectively. The wall proximity and the displacement corrections recommended by [21] and [22] were adopted in the current

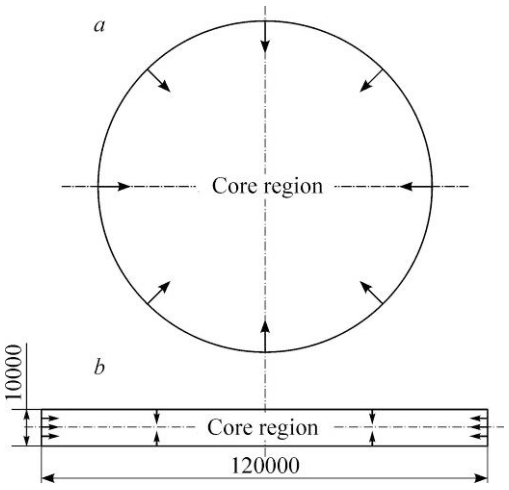

Fig. 8. Schematic for (*a*) the pipe and (*b*) the channel cross sections.

Table 1

Summary of the pipe log-law constants for $R^+ = (Ru_\tau/\nu) = 5673–8652$ and different log ranges utilizing the pressure probe results.

Log range $y^+ = (y^+_{\text{inner}} - y^+_{\text{outer}})$	Hot wire		Pressure probe					
			Without correction		Correction approach [21]		Correction approach [22]	
	κ	B	κ	B	κ	B	κ	B
$y^+ = 30 - 0.15\,R^+$	–	–	0.434	6.34	–	–	–	–
$y^+ = 150 - 0.15\,R^+$	0.384	4.43	0.3955	4.78	0.30	4.67	0.388	4.60

Table 2

Summary of the channel log-law constants for $R^+ = (Hu_\tau/2\nu) = 1014–4816$ and different log ranges utilizing the pressure probe results.

Log range $y^+ = (y^+_{\text{inner}} - y^+_{\text{outer}})$	Hot wire		Pressure probe					
			Without correction		Correction approach [21]		Correction approach [22]	
	κ	B	κ	B	κ	B	κ	B
$y^+ = 30 - 0.2\,R^+$	—	—	0.414	5.42	—	—	—	—
$y^+ = 150 - 0.2R^+$	0.37	3.7	0.385	4.43	0.373	3.89	0.373	3.85

paper. To account for the shear gradient effect, [22] introduced a correction factor for the pressure probe measurements by shifting the wall vertical coordinates by $\Delta = 0.15\,d_0$ towards the higher velocity region, where Δ is called a displacement correction factor. Therefore, it seems at first glance that it is easy to correct the pressure probe data for the shear gradient effect by adding $0.15\,d_0$ to the y-coordinates. However, this displacement correction is dependent not only on the probe outer diameter but also on the magnitude of the velocity gradient and the distance from the wall. Therefore, to avoid the constant shift for the probe data measured, [29] and [30] proposed a modified displacement correction (ε) as a function of the probe outer diameter, d_0 and the local velocity gradient, dU/dy, which reads as

$$\varepsilon = \frac{\Delta}{d_0} = 0.15\,\tanh(4\sqrt{\alpha}) \tag{4}$$

that to be applied for $y > 2d_0$, where the shear parameter α is given by

$$\alpha = d_0\,\frac{dU/dy}{2U} \tag{5}$$

and evaluated at the geometric centre of the pressure probe. Here α is to be determined using the mean-velocity gradient, dU/dy, either calculated from the uncorrected velocity measured or from an iterative scheme proposed by [21] both using the three-point differentiation scheme [31].

In addition to the displacement correction discussed above, an additional correction for the wall proximity effect was also carried out for wall distances less than $2\,d_0$ from the wall. The mechanism of the wall proximity effect on the pressure probe readings was explained by [24] as it resembles a forward-facing step. When the pressure probe approaches the wall, flow blockage occurs, causing the streamlines to be displaced away from the wall towards the region of the higher velocity. For wall distances $y < 2\,d_0$, [22] observed the wall proximity effect on the pressure probe measurements, and, therefore, proposed a correction curve presented in Fig. 8 in his paper in the form of $\Delta U/U = f(y/d_0)$. Based on the wall correction curve by [22], the so-called velocity correction (i.e., the wall term) was proposed by [24], accounting for the wall-proximity and turbulence effects, taking the following form:

$$\Delta U/U = 0.015\exp\left[-3.5((y/d_0) - 0.5)\right]. \tag{6}$$

It is applied to correct the velocity measured for wall distances $y < 2\,d_0$.

For the shear gradient or the displacement effect, [21] suggested an alternative near-wall correction method for $y < 3d_0$, taking the following form:

$$\left[\Delta/d_0\right]_{\text{revised}} = 0.15 \tanh\left(4\sqrt{\alpha}\right) - \varepsilon_{\text{new}} \tag{7}$$

Equation (7) is a revised version for the former displacement correction (ε) presented in equation (4), however, to be applied for wall distances $y < 3d_0$, where

$$\varepsilon_{\text{new}} = \beta_1 \left(y/d_0 - 3\right) + \beta_2 \left(y/d_0 - 3\right)\left[0.15 \tanh(4\sqrt{\alpha})\right] \tag{8}$$

Here β_1 = 0.174 and β_2 = –1.25. It is to note that the correction embodied in (7) was recommend by [21] for the near-wall effect when the probe outer diameter is $d_0^+ < 150$. The correction relation revisited, i.e., equation (7), was also adopted and applied to the current pipe and channel measurements, accounting for the near-wall blockage effect, i.e. for $y < 3\ d_0$, and compared with the near-wall correction proposed by [22] and recently by [24], i.e., equation (4).

It is worth to re-note here that the outer diameters of the pressure probes utilized in the present study were 0.6 mm, and 1 mm which were equivalent to $d_0^+ \approx$24–116 in terms of the wall units for the current working range of Reynolds number. It appears from Fig. 9*a* and 9*b* that for wall distances y^+<300, the pressure probe data suffers from both the wall proximity and the shear gradient effects. Corrections discussed above for the wall proximity and the shear gradient effects are therefore applied to the current pipe and channel flow measurements and selected samples from the data corrected are presented in Fig. 9*a* and 9*b*. To make the comparison among the various corrections more clear, the selected corrected samples presented in these figures for the pipe and the channel flows, respectively, are compared with the uncorrected data. In the figure, the raw and corrected pressure probe data are also compared with the hot-wire data. For the displacement effect, the revisited displacement correction (ε) [i.e. equation (4)] is compared with the correction proposed by [22] for the shear gradient effect. A successful correction approach is usually to be judged by having a good collapse of the pressure probe data corrected with the hot-wire measurements. The near-wall correction proposed by [21] is compared with the original near-wall velocity correction suggested by [22] and both data corrected are presented in Fig. 9*a* and 9*b*. The outcomes with [21] correction method seems to be in good agreement with data corrected applying the near-wall correction approach of [22]. A general conclusion by looking at Fig. 9*a* and 9*b* might be drawn that the pressure probe corrected data have plausible agreement with the hot-wire data. However, it becomes a critical issue, in particular, with the consideration of specifying the inner limit of the logarithmic velocity profile, taking into account the data points within the $2d_0$ from the wall (equivalent to $y^+ \le 300$). When the experimental data uncorrected for wall distances $y^+ < 300$ was used in the analysis of the logarithmic velocity profile, few concerns arose. For instance, utilizing the present data uncorrected while considering the inner limit of the logarithmic line to be y^+=30, which was the most common inner limit for few decades before 1990s, results in κ = 0.434, B = 6.34 for the pipe and κ = 0.414, B = 5.42 for the channel which are not surprising to be in close agreement with the most earlier accepted values in fluid mechanics community κ = 0.417 and B = 5.84 or κ = 0.4 and B = 5.0 [12]. On the contrary, based on recent analysis of the logarithmic law of the wall (see, e.g., [21, 24, 25]), considering the inner limit to be $y^+ \approx 300$ for the pipe flow, new values for both constants of the logarithmic line were obtained, see Table 1 and Table 2, showing good agreement with recent values obtained by [16, 21, 25]. One might also observe from Fig. 9 that the collapse of the data obtained utilizing the pressure probes indicates the good capabilities of the correction methods adopted in this piece of work. More analysis of the experimental data presented in Figs. 6–9 results in useful outcomes which are summarized and presented in Tables 1 and 2. One might observe from data summarized in both Tables 1 and 2 that the inner limit of the logarithmic line plays a major role in estimating its constants.

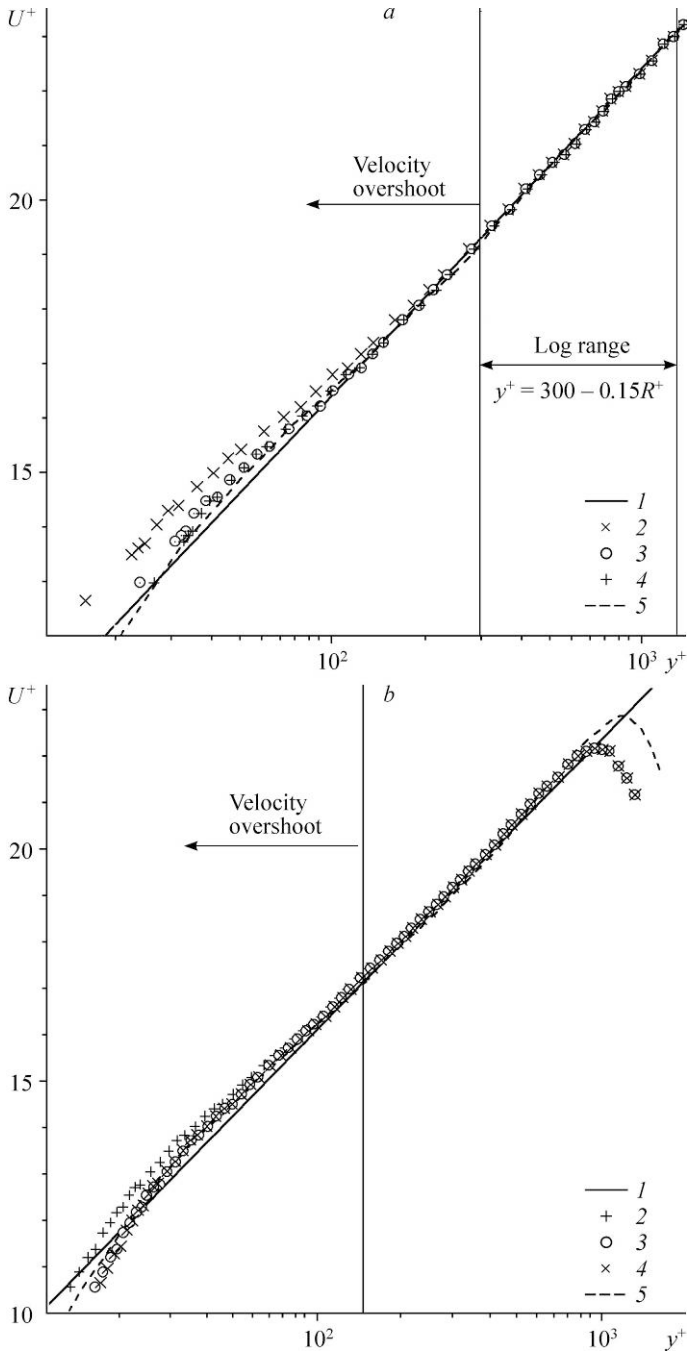

Fig. 9. Corrected versus uncorrected pressure probe mean velocity profiles compared with the logarithmic line and the hot wire data in (*a*) the pipe flow and in (*b*) the channel flow, correction 1 is based on [21] and correction 2 is based on [22].

1 — logarithmic line: $k = 0.384$, $B = 4.43$ (*a*), $k = 0.37$, $B = 3.7$ (*b*);

2 — Pitot data, uncorrected: $R^+ = 8652$ ($d_0^+ = 70$) (*a*), $R^+ = 1014$ ($d_0^+ = 24$) (*b*);

3 — Pitot data, correction 1: $R^+ = 8652$ ($d_0^+ = 70$) (*a*), $R^+ = 1014$ ($d_0^+ = 24$) (*b*);

4 — Pitot data, correction 2: $R^+ = 8652$ ($d_0^+ = 70$) (*a*), $R^+ = 1014$ ($d_0^+ = 24$) (*b*);

5 — hot wire data: $R^+ = 8509$ (*a*), $R^+ = 1167$ (*b*).

Conclusions and final remarks

Accurate measurements utilizing both the pressure probe and the hot wire have been carried out in two different facilities at LSM and LAS for relatively high Reynolds numbers. Pressure probe results, uncorrected and corrected for the wall proximity and the shear gradient effects, were presented and compared with the results obtained using the hot-wire anemometer. The conclusions drawn from the results discussed in the different sections may be summarized as follows.

Corrections for the viscous effect were neglected since the lowest Reynolds number value for the present measurements was beyond the upper limit, i.e. $\mathrm{Re}_p = 200$, assumed for neglecting the viscous effect. The correction for the viscous effect is usually to be taken into consideration when $30 < \mathrm{Re}_p < 200$ [20].

A revisited near-wall correction by [21] has been implemented, providing results that are similar to those obtained using the near-wall correction proposed by [22].

Separate corrections for the streamwise turbulent velocity fluctuations were not conducted since corrections for the turbulence effects are embedded in the near-wall correction in equation (6).

A proper correction for both the wall proximity and the shear gradient effects indicated that the pressure probe can be utilized for measuring the mean velocity distribution, providing data comparable to those measured by the hot-wire anemometer.

The corrected data were 1.5 % in agreement with the hot-wire measurements.

Further study at higher values of the Reynolds numbers, however, is needed to further understand the effect of the pressure probe corrections on the scaling laws and on values of the constants of the logarithmic velocity profile. It is also worth paying more attention to measuring techniques such as the laser Doppler anemometry that would help more resolving the wall layer of the wall-bounded shear flows with better resolution, remedying the unsatisfactory situation with pressure probes measurements even in case they are to be used with small diameters.

The authors gratefully acknowledge the support received from both the Institute of Fluid Mechanics (LSTM), Erlangen-Nürenberg and the Department of Aerodynamics and Fluid Mechanics (LAS), BTU-Cottbus.

Nomenclature

B — log law additive constant ,
c_f — channel skin friction coefficient,
D — pipe diameter, m
d — hot-wire diameter/static pressure tap diameter, m,
d_0 — pressure probe outer diameter, m,
d_{in} — pressure probe inner diameter, m,
dP/dx — mean pressure gradient, Pa/m,
H — channel full height, m,
l/l_c — hot-wire length/flow characteristic length, m,
L — length of the pipe/channel test section, m,
R — pipe radius, m,
R^+ — Kármán number,
Re — Reynolds number,
$\bar{U}$ — fluid bulk/mean velocity, m/s,
u_τ — wall friction velocity, m/s,
W — channel width, m,
y — distance to the wall, m.

Geek symbols

τ — shear stress, N/m^2,
λ — pipe friction factor,
ν — fluid kinematic viscosity, m^2/s,
κ — von Kármán constant,
ρ — fluid density, kg/m^3,
Δ — centerline offset/displacement correction, m,
δ — boundary layer thickness, m.

Subscripts

b — bulk, c — characteristics, w — wall, p — probe, m — mean, + — dimensionless.

References

1. **F. Zimmer, E.-S. Zanoun, and C. Egbers,** A study on the influence of triggering pipe flow regarding mean and higher order statistics, J. Physics: Conf. Series, 2011, Vol. 318, No. 3, P. 32039–32044.
2. **E.-S. Zanoun, F. Durst, and H. Nagib,** Refined C_f relation for turbulent channels and consequences for high Re experiments, J. Fluid Dyn. Res., 2009, Vol. 41, No. 2, P. 021405-1–021405-12.
3. **F. Durst and E.-S. Zanoun,** Experimental investigation of near-wall effects on hot-wire measurements, Exp. Fluids, 2002, Vol. 33, No. 1, P. 210–218.
4. **F. Zimmer, E.-S. Zanoun, and C. Egbers,** The CoLaPipe — the new Cottbus large pipe test facility at BTU Cottbus, Review Scientific Inst., 2014, Vol. 85, No. 7, P. 075115-1–075115-9.
5. **E.-S. Zanoun, M. Kito, and C. Egbers,** A study on flow transition and development in circular and rectangular ducts, J. Fluids Engng, 2009, Vol. 131, No. 6, P. 061204-1–061204-10.
6. **D.W. Bryer and R.C. Pankhurst,** Pressure-probe methods for determining wind speed and flow direction, Nat. Phys. Lab., London, 1971.
7. **S. Sami,** The Pitot tube in turbulent shear flow, in: Proc. 11th Midwestern Mech. Conf., Dev. in Mechanics, 1967, Vol. 5, P. 11. P. 71.
8. **S.H. Chue,** Pressure probes for fluid measurements, Pro. Aero. Sci., 1975, Vol. 16, No. 2, P. 147–223.
9. **B.J. McKeon and A.J. Smits,** Static pressure correction in high Reynolds number fully developed turbulent pipe flow, Meas. Sci. Technol., 2002, Vol. 13, No. 10, P. 1608–1614.
10. **L. Prandtl,** Reibungswiederstand, hydrodynamische Probleme des Schiffsantriebs, herausgeg. von G. Kempf und E. Förster, Hamburg, 1932. S. 87. Neuere Ergebnisse der Turbulenzforschung, Z. VDI Bd. 77, Nr. 5, S. 105–113; Ergebnisse der Aerodynamischen Versuchsanstalt Göttingen, 3 Lief. 1927. S. 1 (English Translation NACA TM 720).
11. **P. Blasius,** Über Flüssigkeitsbewegung bei sehr kleiner Reibung, in: Proc. Third Int. Math. Congr. Heidelberg, 1908, P. 484–491.
12. **J. Nikuradse,** Gesetzmässigkeiten der turbulenten Strömung in glatten Rohren, Forschg. Arb. Ing.-Wes., 1932, No. 356, P. 1–36.
13. **B.J. McKeon, J. Li, W. Jiang, J.F. Morrison, and A.J. Smits,** A new friction factor relationship for fully developed pipe flow, J. Fluid Mech., 2005, Vol. 538, P. 429–443.
14. **P. Bradshaw and G.E. Hellens,** The N.P.L. 59 in × 9 in boundary layer tunnel, NPL Aero Report, 1964, No. 1119.
15. **R.B. Dean,** Reynolds number dependence of skin friction and other bulk flow variables in two dimensional rectangular duct flow, Phys. Fluids, 1978, No. 100, P. 215–223.
16. **I. Marusic, B.J. McKeon, P.A. Monkewitz, H.M. Nagib, A.J. Smits, and K.R. Sreenivasan,** Wall-bounded turbulent ows at high Reynolds numbers: Recent advances and key issues, Phys. Fluids, 2010, Vol. 22, No. 6, P. 065103-1–065103-24.
17. **J.P. Monty,** Developments in smooth wall turbulent duct flows, PhD thesis, The University of Melbourne, Australia, 2005.
18. **K.T. Christensen,** Experimental investigation of acceleration and velocity fields in turbulent channel flow, PhD thesis, University of Illinois at Urbana-Champaign, Department of Theoretical and Applied Mechanics, USA, 2001.
19. **F. Durst, H. Kikura, I. Lekakis, J. Jovanovic, and Q.-Y. Ye,** Wall shear stress determination from near-wall mean velocity data in turbulent pipe and channel flows, Exp. Fluids, 1996, Vol. 20, No. 6, P. 417–428.
20. **W.I. Grosser,** Factors influencing pitot probe centerline displacement in a turbulent supersonic boundary layer, NASA Technical Memorandum 107341, 1997, P. 1–47.
21. **S.C.C. Bailey, M. Hultmark, J.P. Monty, P.H. Alfredsson, M.S. Chong, R.D. Duncan, J.H.M. Fransson, N. Hutchins, I. Marusic, B.J. McKeon, H.M. Nagib, R. Orlue, A. Segalini, A.J. Smits, and R. Vinuesa,** Obtaining accurate mean velocity measurements in high Reynolds number turbulent boundary layers using Pitot tubes, J. Fluid Mech., 2013, No. 715, P. 642–670.
22. **F.A. MacMillan,** Experiments on Pitot-tubes in shear flow, Aero. Res. Counc. R. & M., 1956, No. 3028.
23. **S. Tavoularis,** Techniques for Turbulence Measurements. Vol. 1. Flow Phenomena and Measurement, Encycl. Fluid. Mech., 1986, P. 1207–1255.
24. **B.J. McKeon, J. Li, W. Jiang, J.F. Morrison, and A.J. Smits,** Pitot probe corrections in fully developed turbulent pipe flow, Meas. Sci. Technol., 2003, Vol. 14, No. 8, P. 1449–1458.
25. **E.S. Zanoun, F. Durst, O. Saleh, and A. Al-Salaymeh,** Wall skin friction and mean velocity profiles of fully developed turbulent pipe flows, Exp. Therm. Fluid Sci., 2007, Vol. 32, No. 1, P. 249–261.
26. **T. Wei and W.W. Willmarth,** Reynolds number effects on the structures of a turbulent channel flow, J. Fluid Mech., 1989, Vol. 204, P. 57–95.
27. **M.V. Zagarola and A.J. Smits,** Mean-flow scaling of turbulent pipe flow, J. Fluid Mech., 1998, Vol. 373, P. 33–79.
28. **M. Fischer,** Turbulente wandgebundene Strömungen bei kleinen Reynoldszahlen, Dissertation. Universität Erlangen Nürnberg, 1999.
29. **M.I. Hall,** The displacement effect of a sphere in two-dimensional shear flow, J. Fluid Mech., 1956, Vol. 1, P. 142–62.
30. **M.J. Lighthill,** Contributions to the theory of the Pitot-tube displacement effect, J. Fluid Mech., 1957, Vol. 1, P. 493–512.
31. **C. Grossmann and H.G. Roos,** Numerik der partiellen Differentialgleichungen, B.G. Teubner, Stuttgart, 1994.